

# A Variable-step Grey Prediction Algorithm on the Synchronous Control for TBM Propulsion System

Hanbing Zhang, Haiguang Zhang, Gang Mu, and Xiuchen Li

**Abstract**—The bond graph theory has been used to construct a mathematical model that addresses the mechanical-electrical-hydraulic coupling features of the TBM propulsion system. This method addresses the drawbacks of the traditional multi-energy domain modeling technique. The TBM propulsion system's state-space representation is obtained, and a synchronized control model is created. To address the issue of traditional PID control's incapacity to attain ideal synchronization control precision, a variable step adjustment algorithm has been presented, based on the grey prediction model. Using MATLAB, the synchronization control of the TBM propulsion system was simulated. The outcomes showed that, when compared to the traditional PID control approach, the gray predictive PID control system improved the synchronization accuracy. The synchronization error of the hydraulic cylinder was reduced from 0.3 mm to 0.15 mm, and the fluctuation of the branch pressure was also reduced. The accuracy of the model has been confirmed through experimental testing.

**Keywords**—TBM, bond graph, synchronization control, grey prediction, step adjustment

## I. INTRODUCTION

Tunnel boring machine (TBM) is a kind of technology intensive engineering equipment specially applied to tunnel construction (railway, highway, water conservancy, municipal construction, etc.). Compared with the traditional drilling and blasting method, TBM, which is environmentally friendly, has advantages of high quality, high efficiency, safety, and low cost. It has become the preferred equipment for tunnel construction [1]. The propulsion mechanism is the core transmission mechanism for TBM to achieve continuous cyclic boring operation. The performance has a great impact on the efficiency and accuracy of the tunneling boring process. The TBM propulsion system is a typical mechanical-electrical-hydraulic

Manuscript received April 18, 2024; revised March 1, 2025.

This work was supported by The National Basic Research Program Of China (973 Program) under grant number [2013CB035403] and the Open Research Fund of Key Laboratory of Environment Controlled Aquaculture, Ministry of Education, China under grant number [202212].

Hanbing Zhang is a lecturer of Mechanical and Power Engineering Department, Dalian Ocean University, Dalian, 116023 China (e-mail: hanbingtbm@yeah.net).

Haiguang Zhang is an undergraduate student of Mechanical and Power Engineering Department, Dalian Ocean University, Dalian, 116023 China (e-mail: jjyao979@163.com).

Gang Mu is a senior experimentalist of the R&D Center of Fisheries Equipment and Engineering, Liaoning Province, Dalian, 116023 China (e-mail: mugang@dou.edu.cn).

Xiuchen Li is a professor of Mechanical and Power Engineering Department, Dalian Ocean University, Dalian, 116023 China (corresponding author, e-mail: liuyz1090@163.com).

system [2],[3]. However, the traditional kinetic analysis method is often limited to a single energy domain system, which has limitations on systems with multiple energy domains. In contrast, the bond graph theory can achieve unification of multi-energy domains, facilitate unified model of multi-energy domains coupling problem and dynamic characteristic analysis research [4].

The traditional PID control strategy has low accuracy in synchronous control of the propulsion system and cannot meet engineering needs. The main reason is that the TBM propulsion system is a typical electromechanical hydraulic coupling system, and the physical phenomena of mechanical, electrical, and hydraulic interactions make the control more complex. As the main component of the propulsion system, the electro-hydraulic proportional pressure reducing valve has nonlinear factors such as hysteresis and dead zone in the valve body [5],[6], and its structural parameters are unclear and have strong time delay. The hydraulic system is significantly affected by changes in temperature, load and other parameters. When precise pressure control is required, closed-loop feedback correction of the outlet pressure is needed for the electro-hydraulic proportional pressure reducing valve. Therefore, conventional control algorithms based on precise mathematical models of the controlled object are difficult to achieve precise synchronous control of the electro-hydraulic proportional system.

The grey prediction algorithm is particularly suitable for systems with unknown parameters, insufficient information, and unclear environmental parameters [7]. Numerous engineering issues have been effectively resolved by the grey prediction algorithm, such as the position and velocity control of FAST hydraulic actuators, robot position control, position control of piezoelectric actuators with built-in hysteresis characteristics[8]-[12].

In this paper, taking a certain type of open TBM propulsion system as the research object, the bond graph model of the system is built. A variable-step grey prediction PID (SGPID) control algorithm is proposed, and an experimental platform is built for experimental verification.

## II. TBM PROPULSION SYSTEM

Fig. 1 shows a schematic illustration of the tunneling conditions for the TBM propulsion system. The system is consists of the surrounding rock, hydraulic drive, and mechanical parts.

Four grouped valve blocks individually regulate the four hydraulic cylinders that activate the propulsion hydraulic system. An electromagnetic reversing valve, a proportional pressure-reducing valve, an auxiliary valve, and the related

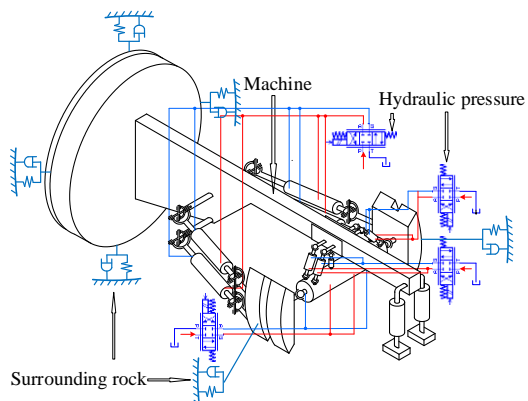


Fig. 1. An illustration of the TBM propulsion system.

detection components are all included in each identical group of control modules. In order to simplify modeling, one of the previously indicated groups will be selected. The schematic diagram for the propulsion hydraulic system simulation with a single cylinder is shown in Figure 2. Primarily, hydraulic system simulation examines the dynamic interplay of motors, gear pumps, hydraulic cylinders, proportional pressure reducing valves, and loads.

Each group of control modules is identical and comprises an electromagnetic reversing valve, a proportional pressure-reducing valve, an auxiliary valve and associated detection elements. Consequently, one of the aforementioned groups may be chosen in order to simplify modeling. Figure 2 illustrates the schematic of the single cylinder simulation of the thrusting system. Hydraulic system simulation mainly analyzes the dynamic relationship between motors, gear pumps, proportional pressure reducing valves, hydraulic cylinders, and loads [15].

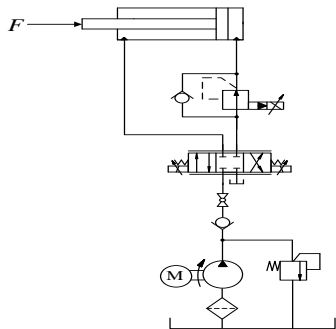


Fig. 2. The simplified simulation schematic of propulsion hydraulic system.

### III. ESTABLISHMENT OF THE SIMULATION MODEL FOR THE PROPULSION SYSTEM

The bond graph models of each subsystem were established first, and then they were combined together to create the bond graph model of the complete system. The hydraulic system's components, including the stepper motor, quantitative gear pump, and hydraulic cylinder, were simulated and modeled. Figure 3 illustrates the system's primary power flow direction and its causal link. A. Model of the Three-phase Motor

With its nonlinear and multi-field interaction, the three-phase motor is a complicated system. [16],[17]. The following simplifications are made to make future modeling and study easier: (1) The three-phase windings are symmetrical, harmonics are disregarded, and the magnetic potential is distributed sinusoidally throughout the gap's circular space; (2) Magnetic saturation is disregarded, and the three windings' mutual and self-inductances are linear; (3) Iron loss, hysteresis, and eddy current loss are disregarded; and (4) the impact of temperature and frequency variations on the windings is not taken into account.

Figure 4(a) shows a commonly used equivalent circuit that describes the physical characteristics of each motor component. The motor is responsible for converting electrical energy into mechanical energy. The circuit portion of the motor, which comprises an equivalent internal resistance connection and an equivalent inductance link, and the right side represents the mechanical rotating part of the motor, with the output shaft's moment of inertia and motor output shaft friction loss being represented by the loss and mechanical loss on power, the bond graph model of the motor is presented in Fig. 4(b).

It can be learned that  $MSeI$  represents the input force variable (the stator voltage  $U_A$  on the A-axis of the motor),  $k_e$  represents the proportional coefficient between the electromagnetic torque and the current (the armature coefficient or torque coefficient,  $k_e = z_r \Phi_m$ ),  $GY$  represents the rotator that transforms electrical energy into mechanical force,  $R_f$  represents the motor friction internal resistance,  $T_{out}$  represents the motor shaft end output torque, and  $\omega_{out}$  represents the output angular velocity of the motor.

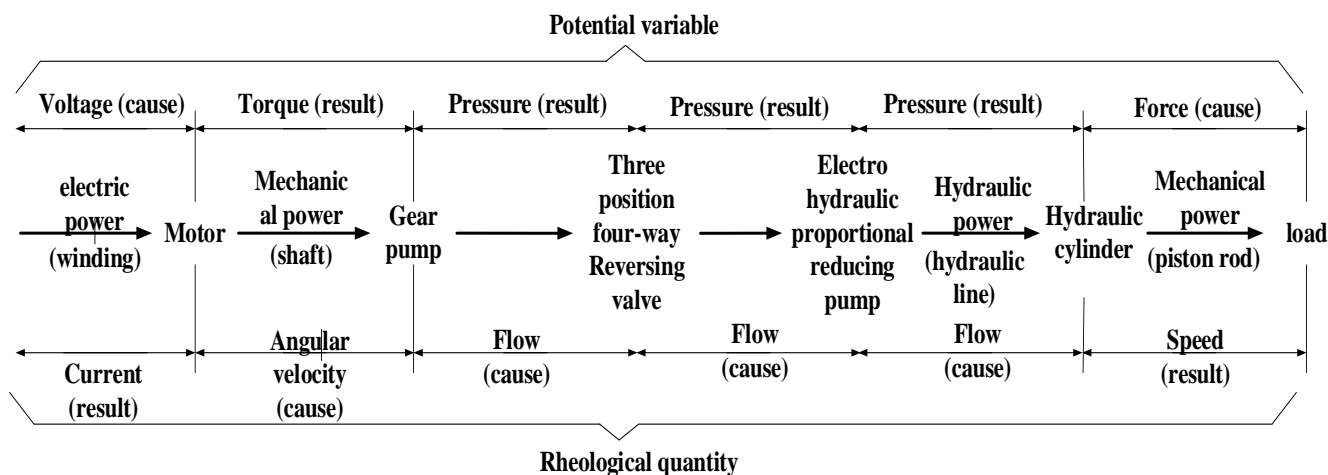


Fig. 3. Power flows of the propulsion hydraulic system.

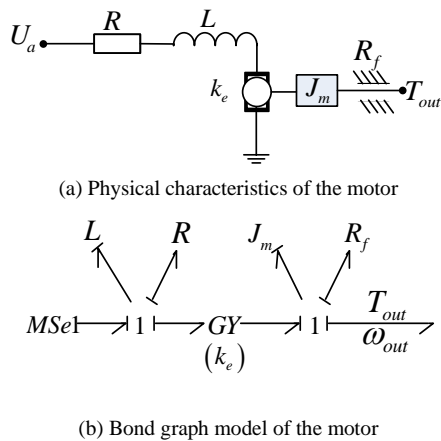


Fig. 4. Mathematical model of three-phase AC asynchronous motor.

**B. Mathematical Model of External-Meshing Quantitative Gear Pump**

Fig. 5 illustrates the external gear pump's operation. The flow and pressure of the oil inlet and outlet of the gear pump are  $P_{in}$ ,  $Q_{in}$ ,  $P_{out}$  and  $Q_{out}$  respectively.  $\Delta P$  represents pressure difference,  $T$  represents the actual input torque,  $n$  represents the pump's speed, and  $V$  stands for the pump's displacement. In this hydraulic system, the pressure of the oil inlet is  $P_{in} = 0Pa$ ; the external gear pump is driven by the two-phase hybrid stepping motor, and the equal flow is achieved through gear meshing output, converting mechanical energy into hydraulic energy of the working fluid [18].

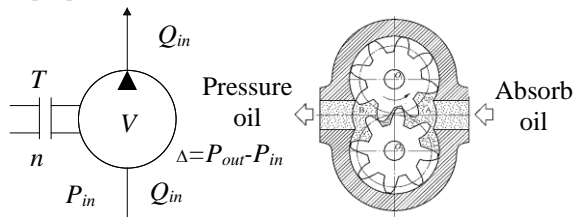


Fig. 5. The schematic diagram of external gear pump.

Comprehensively considering the factors affecting the flow and torque of the external gear pump, the bond graph model of the gear pump is shown in Fig. 6, where  $MSe2$  represents the force variable (torque) input to the gear pump,  $TF1$  represents the converter that converts mechanical power to hydraulic power,  $R_w$  represents the internal resistance due to the loss of rotational resistance of the pump, and  $\omega_{in}$  represents the angular velocity of the gear pump.

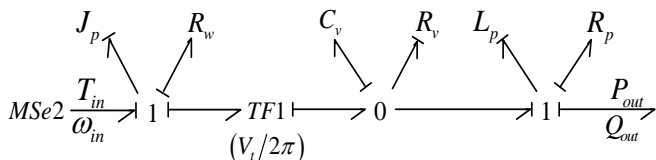
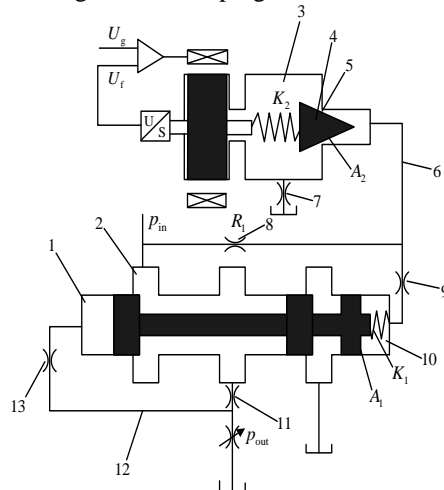


Fig. 6. Bond graph of external-meshing quantitative gear pump.

**C. Model of Proportional Pressure Reducing Valve**

The operation of the proportional pressure reduction valve is demonstrated in Fig. 7. The system is divided into two subsystems: the pilot valve subsystem, which has a proportional solenoid, and the main valve subsystem. The system is somewhat simplified to make modeling easier, the following presumptions: (1) only the steady-state hydraulic

force is taken into account, ignoring the transient hydraulic force operating on the spool; (2) oil temperature is stable; (3) there is no change in the damping air flow coefficient [19].



1-Chamber C1; 2-Cavity C2; 3-Cavity C5; 4-Guide spool; 5-Damping hole d; 6-Cavity C4; 7-Damping e; 8-Damping hole b; 9-Damping hole c; 10-Cavity C3; 11-Damping hole o; 12-Cavity C6; 13-Damping hole a; 14-Main spool

Fig. 7. The schematic diagram of the pilot proportional valve.

Bond graph models are built for the proportional electromagnetic pilot valve subsystem and the main valve subsystem separately. The bond graph model of the proportional pressure reduction valve is then created by integrating the two models, as shown in Figure 8.

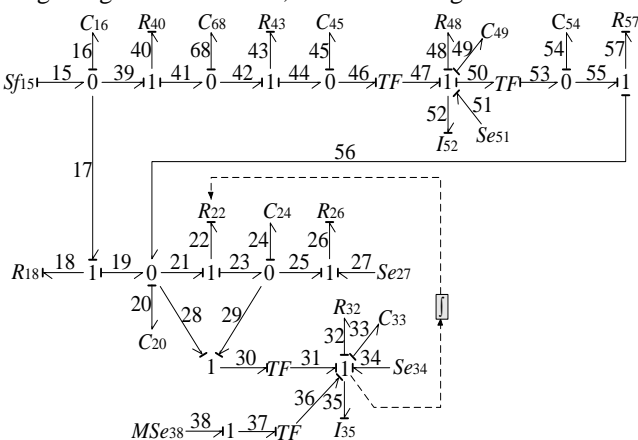


Fig. 8. Bond graph model of proportional pressure reducing valve.

**D. Model of Asymmetric Hydraulic Cylinder**

The asymmetric hydraulic cylinder is assumed to have the following three characteristics: (1) pipeline dynamics and fluid quality effects are disregarded; (2) the hydraulic cylinder's external and internal leaks are both in a laminar flow state.; (3) since the pressure in the hydraulic cylinder is constant throughout, the cavity's liquid will not be saturated and cavitation will not occur. [20].

Figure 9 displays the schematic diagram for the asymmetric hydraulic cylinder.  $F$  represents the output force on the piston rod,  $v_p$  represents the speed of the piston rod,  $P_1$  and  $P_2$  represent the oil pressure in the rodless cavity and the rod cavity,  $Q_1$  and  $Q_2$  represent the oil flow rate of rodless cavity and the rod cavity, and  $A_1$  and  $A_2$  A stands for both the rod cavity and the rodless cavity's effective working area.

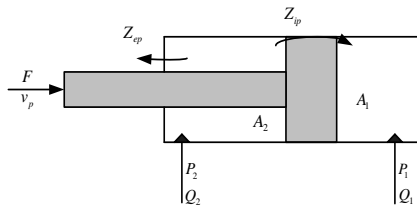


Fig. 9. The schematic diagram of asymmetric hydraulic cylinder.

Figure 10 shows the model of the asymmetric cylinder, taking into account the piston rod, the viscous damping friction of the load, the total leakage, and the compressibility of the hydraulic fluid.

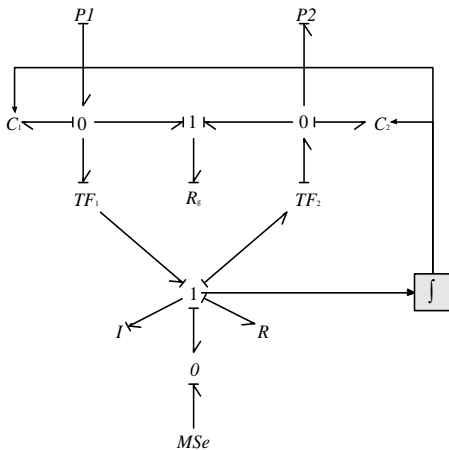


Fig. 10. Model of asymmetric cylinder.

E. State Equation of the Propulsion System

As seen in Fig. 11, a comprehensive bond graph model of the propulsion system can be created by combining the aforementioned subsystem models. The model of the system makes it simple to determine the state equation of the system, which makes it easier to conduct further study on synchronous control of the propulsion system. With input variable  $U(t)$  and output variable  $Y(t)$ , the system is a six-input single-output system, according to analysis. There are sixteen energy storage components in the system, which are corresponding to state variable  $X(t)$ .

$$U(t) = [MSe_1 \ Se_{27} \ Se_{34} \ Se_{38} \ Se_{51} \ Se_{64}]^T$$

$$Y(t) = [v_p]$$

$$X(t) = [p_2 \ p_6 \ p_{13} \ q_{33} \ q_{49} \ p_{62} \ q_{10} \ q_{16}$$

$$q_{20} \ q_{24} \ p_{35} \ q_{45} \ p_{52} \ q_{54} \ q_{59} \ q_{68}]^T$$

The following is a list of energy storage element's flow and potential equations based on the causal relationship and power flow direction.

The state space equation of the system is:

$$\begin{cases} \dot{X}(t) = A(t) \cdot X(t) + B(t) \cdot U(t) \\ Y(t) = C(t) \cdot X(t) + D(t) \cdot U(t) \end{cases}$$

In addition, the state matrix  $A(t)$ , input matrix  $B(t)$ , output matrix  $C(t)$  and direct connection matrix  $D(t)$  are respectively:

$$A(t) = \begin{bmatrix} A_1(t) & A_2(t) \\ A_3(t) & A_4(t) \end{bmatrix}$$

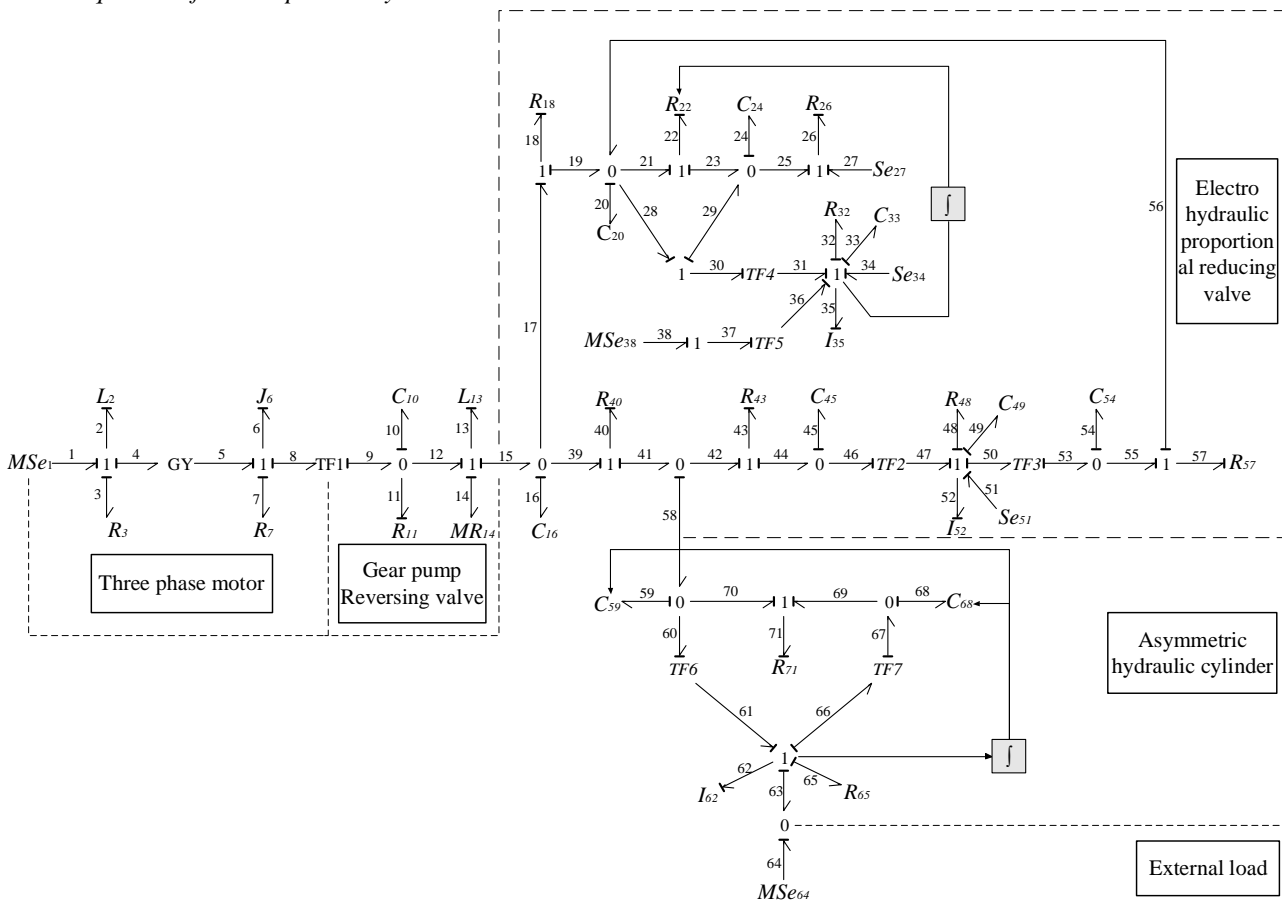
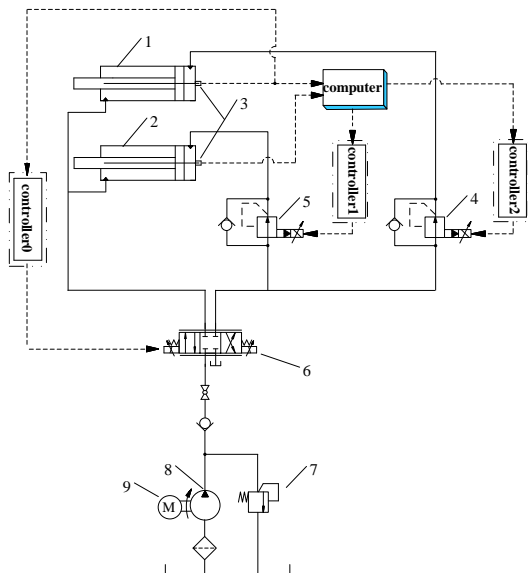


Fig. 11. Bond graph model of hydraulic propulsion system.





1, 2- asymmetric hydraulic cylinder; 3- displacement sensor; 4, 5- electric-hydraulic proportional pressure reducing valve; 6- three-position four-way proportional reversing valve; 7- safety valve; 8- external meshing quantitative gear pump; 9- three-phase AC asynchronous motor  
 Fig. 12. Schematic of propulsion system's position control synchronization.

**B. Computer Simulation Model of Synchronization Control**

As shown in Fig. 13, a computer simulation model of the synchronous control of the previously mentioned propulsion system was created by merging the thrusting system's state

space expression. This model development greatly lowers the computing complexity while also simplifying the mathematical description of the closed-loop system. By optimizing synchronous control algorithm for the propulsion system, the simulation model raises the system response time and control precision. In order to effectively deploy the TBM propulsion system in a variety of geological settings, the model is an essential tool for furthering research and improvements to the system.

**V. VARIABLE-STEP GREY PREDICTION PID CONTROL**

The innovation with equal dimensions, the data is updated using the GM (1,1) model, which also predicts the next output value of the system based on sampling time  $t$  and historical data produced by the system in earlier steps. The prediction error  $e(t)$  and prediction error rate of change  $ec(t)$  are computed and used as the foundation for adjusting the PID controller parameters  $K_p$ ,  $K_i$ , and  $K_d$ . The control performance of the grey prediction PID controller is significantly impacted by the prediction step size  $m$ . A mechanism to dynamically modify the prediction step size in accordance with the actual error  $E(t)$  and the error change rate  $EC(t)$  of the system at the current moment is introduced in order to further enhance the controller's performance. Figure 14 illustrates the SGPID controller's working principle.

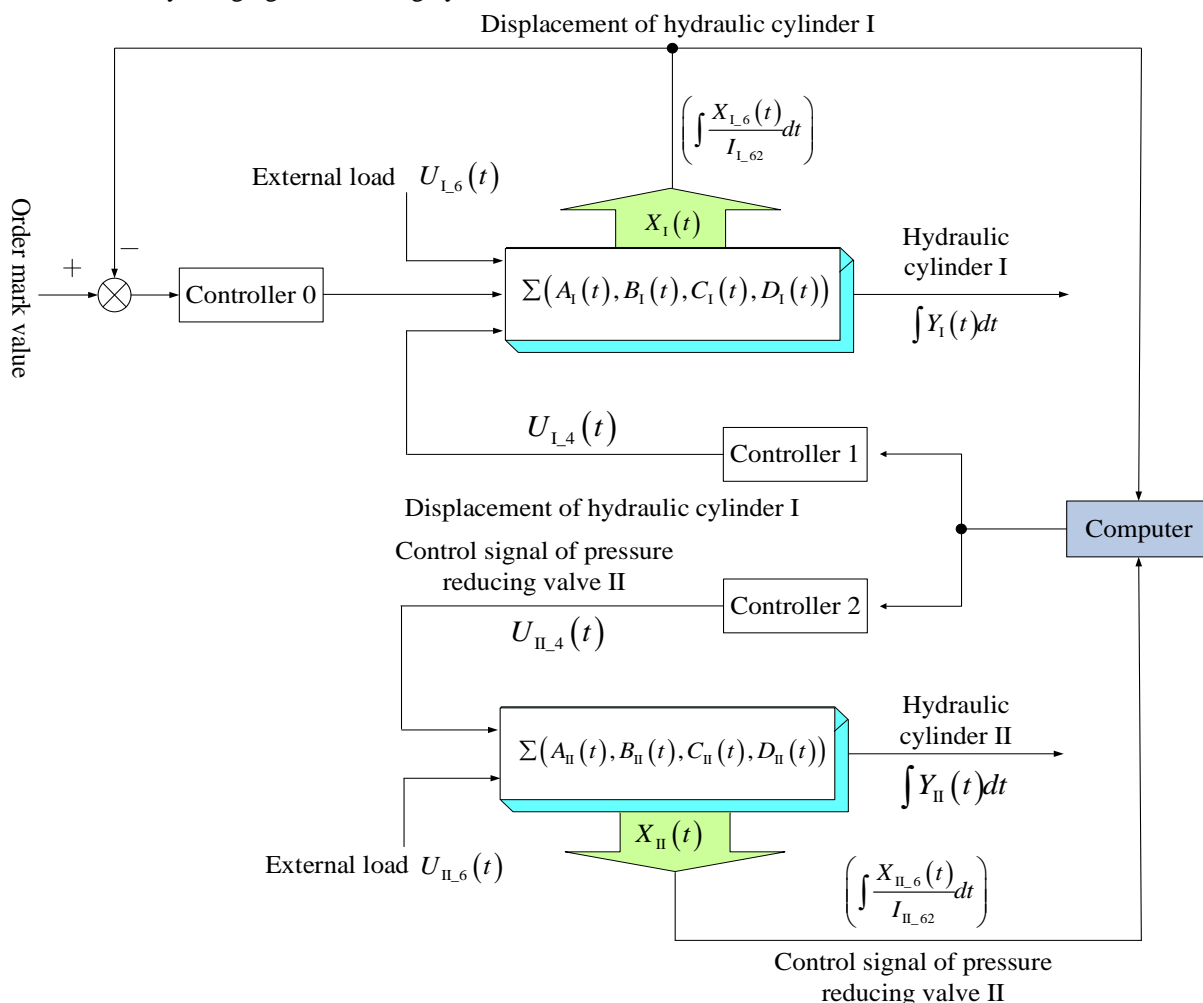


Fig. 13. Computer simulation model for synchronous control of propulsion system.

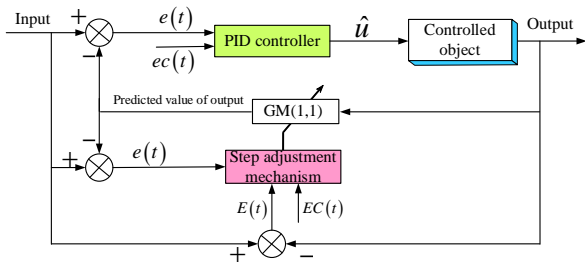


Fig. 14. Schematic diagram of SGPID.

A. The New Step Adjustment Mechanism

Currently, there are primarily two approaches to step adjustment: (1) creating intricate step size adjustment using fuzzy rules, which is labor-intensive and time-consuming and necessitates extensive manual experience and on-site testing; (2) a step size transformation threshold is artificially set as the boundary condition for step size adjustment in accordance with engineering requirements. The system is then further divided into three response stages: rising, falling, and stationary (to ascertain whether they are near the set value) by comparing the actual error at time t with the size of the step size transformation threshold. Even though this approach does not require the creation of fuzzy rules, the process of figuring out the step size transformation threshold is extremely intricate, and a threshold that is too big or too little will significantly affect how the response stage will be further divided and the step size will be chosen [26].

The system prediction error  $e(t)$  is added to the step adjustment mechanism's discrimination requirements in this article. The step size is changed and the system's operational stage is accurately identified based on its directional relationship with the real system error  $E(t)$ . At the condition  $e(t)E(t) < 0$ , the fluctuation has changed around the set value. A smaller absolute number for the prediction step size will be chosen to prevent overshoot.

At the condition  $e(t)E(t) \geq 0$ , it shows that the actual error is high and that the system has greatly surpassed the predetermined value. Table 1 displays the particular step adjustment approach.

B. Equal Dimensional Innovation GM (1,1) Model

Given that the sampling value at time  $t$  is  $Y^{(0)}(t)$ , and a sequence  $(Y^{(0)}(t-n+1), Y^{(0)}(t-n+2), \dots, Y^{(0)}(t))$  with the previous data  $n-1$  is formed, then the rolling prediction algorithm of equal dimensional innovation is shown in the following formula, which is the prediction output value of the system  $m$  step.

$$\hat{Y}^{(0)}(t+m) = Y^{(0)}(t-n+1)(1-e^a) \cdot e^{-a(t+m-1)} - \frac{b}{a}(1-e^a)e^{-a(t+m-1)}$$

The formula designates the parameters  $a$  and  $b$  as the grey action quantity and the development coefficient, respectively. Because industrial control demands high real-time performance, the established sequence size should be as small as possible, usually  $n=5$ .

VI. SIMULATION AND EXPERIMENT

A. Simulation Analysis

The control effect of the SGPID and the traditional PID control strategy in the electric-hydraulic proportional synchronization control of the propulsion system was assessed using a MATLAB simulation. Each mechanical component of the TBM has a geometric size reduction factor of 1:10, an external load reduction factor of 1:1000, and a stiffness reduction factor of 1:100. The testing apparatus is built in the upcoming chapters. Each asymmetric hydraulic cylinder's maximum working load throughout the thrusting operation is 5000N. The hydraulic cylinder has an inner diameter of 50 mm, a piston rod diameter of 28 mm, a maximum elongation of

TABLE 1. THE STEP ADJUSTMENT STRATEGY

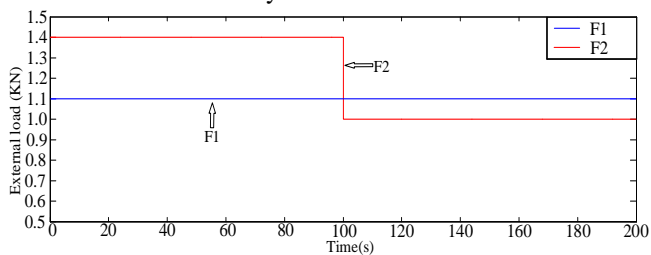
Response phase	Further division	Actual error	Control mode	Predict the step size
ascending phase, $EC < 0$	around the setpoint, $e \cdot E < 0$	approaching the setpoint $E \geq 0$	rise slowly and avoid overshoot	-1
		slightly beyond the setpoint $E < 0$	slow down and avoid oscillations	1
	deviate too much from the setpoint, $e \cdot E \geq 0$	too much below the setpoint $E \geq 0$	rise fast and reduce the rise time	-2
		the setpoint is exceeded too much $E < 0$	drop fast and avoid overshoot	2
descending phase, $EC > 0$	around the setpoint, $e \cdot E < 0$	approaching the setpoint $E \geq 0$	rise slowly and avoid overshoot	-1
		slightly beyond the setpoint $E < 0$	slow down and avoid oscillations	1
	deviate too much from the setpoint, $e \cdot E \geq 0$	too much below the setpoint $E \geq 0$	rise fast and reduce the rise time	-2
		the setpoint is exceeded too much $E < 0$	drop fast and avoid overshoot	2
plateau phase, $EC = 0$	—	fixed value	avoid static errors and oscillations	1

200 mm, a working stroke of 164 mm, a rated pressure of 5 MPa, and a working pressure of 2.5 MPa. There has a displacement of 14ml/min and a speed of 1450r/min. The three-position four-way electromagnetic reversing valve has a rated flow of 4L/min and a rated pressure of 21MPa. The reversing valve's oil return chamber pressure is recorded as 0 MPa during advancement, whereas the inlet pressure is 14 MPa and the exit pressure is unknown but is assumed to be 13.5 MPa. The electric-hydraulic proportional pressure-reducing valve starting pressure is set to 2.5 MPa.

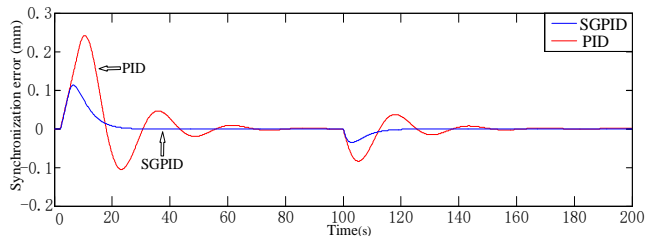
With the same control parameters (controller 0:  $K_{Pw}=22.5$ ,  $K_{Iw}=0.25$ ,  $K_{Dw}=8$ , synchronization controller:  $K_{Pn}=25$ ,  $K_{In}=7$ ,  $K_{Dn}=0.16$ ), the synchronization controllers (controllers 1 and 2) replicate the synchronous performance of the propulsion system using the traditional PID and the SGPID control strategy, respectively, while controller 0 directs the hydraulic cylinder to cease moving when it reaches the position of 10mm. Fig. 15(a) shows the eccentric loading curves for the two hydraulic cylinders..

The external load applied to the two hydraulic cylinders shows a phase shift, F1 and F2 are not the same, according to an analysis of the synchronization error curve in Fig. 15(b). Under the PID control algorithm, the synchronization error is characterized by a slow attenuation of the oscillations and considerable oscillation and overshoot. The SGPID, on the other hand, shows a small overshoot and some oscillation. The overshoot of both control methods grows with step signal amplitude, whereas the synchronization error under SGPID control stays constant and rapidly decreases. While the synchronization error under PID control was within 0.25mm, the synchronization error under SGPID control stayed within 0.12mm over the whole operation..

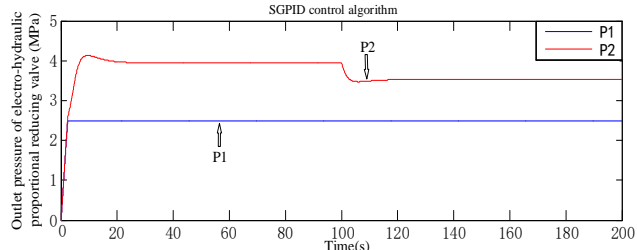
Figures 15(c) and 15(d) show the electric-hydraulic proportional pressure-reducing valve's outlet pressure under the two control schemes of SGPID and PID. The starting adjustment pressure of 2.5 MPa serves as the minimum adjustment standard for the pressure-reducing valve's outlet pressure during the hydraulic cylinder's extension procedure. If, during the synchronization control process, the outlet pressure of one pressure-reducing valve needs to be further reduced after being adjusted to 2.5 MPa, the system will then modify the outlet pressure of the other pressure-reducing valve. This is to make sure the hydraulic cylinder can resist the operation of the maximum external load force. As illustrated in the figure, the outlet pressure of the pressure-reducing valve changes quickly. The SGPID control makes a steady adjustment without oscillation, and has better control efficacy than PID control.



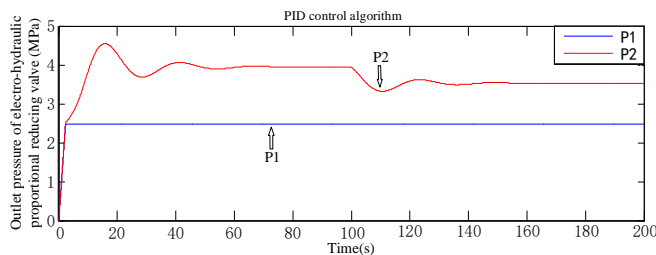
(a) Load loading curve



(b) Synchronization error curves under two control strategies



(c) Outlet pressure of electric-hydraulic proportional pressure reducing valve under SGPID



(d) Outlet pressure of electric-hydraulic proportional pressure reducing valve under PID

Fig. 15. Synchronous simulation under partial load.

**B. Experimental Verification**

Figure 16 depicts the general layout of the TBM experimental prototype. The frame, host, load loading device, and surrounding rock simulation device comprise the primary body of the experimental prototype.

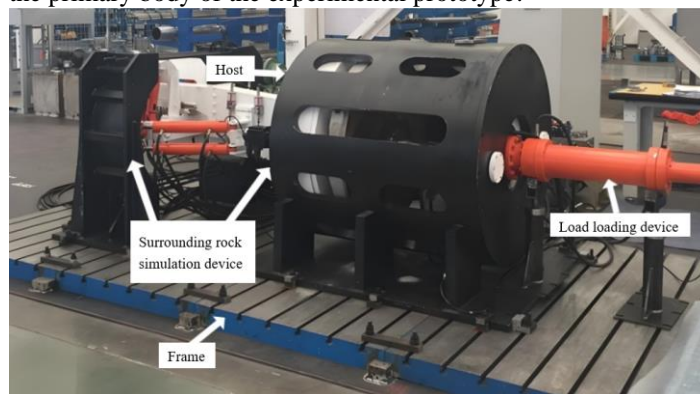
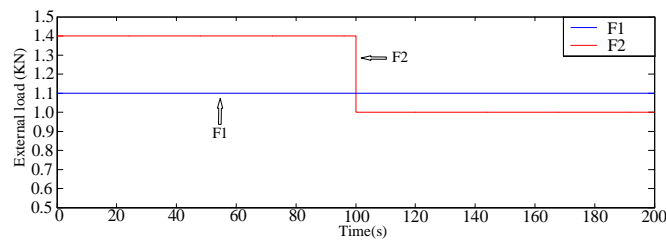


Fig. 16. Experimental prototype.

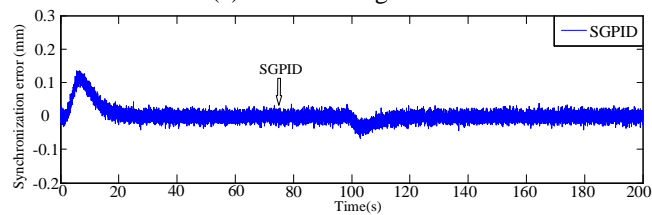
The controller now incorporates both the traditional PID and the SGPID, enabling testing of the thrusting system's synchronization control. Figure 17 (a) displays the partial load loading curves adapted to two hydraulic cylinders, whereas Figure 17(b) and Figure 17(c) shows the corresponding error curves for the two control strategies. Lastly, Figure 17(d) and Figure 17(e) show the outlet pressure curves of the pressure-reducing valve under the two control strategies. The simulated and experimental results are consistent, as shown in Figs. 15 and 17. The largest synchronization error produced by the PID control approach

was 0.3mm, while the synchronization error under SGPID control stayed within 0.15mm during the whole process. The outlet pressure of the pressure-reducing valve shows a significantly low oscillation and more stable pressure regulation under SGPID control, compared to the PID control approach.

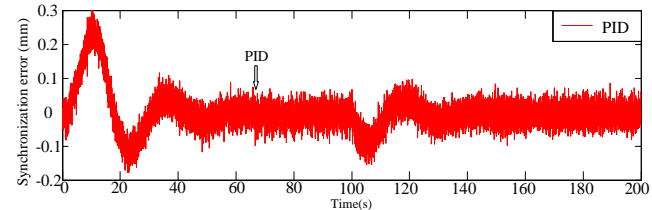
The effectiveness of the control method in question is confirmed by a comparison of the curves in Figures 15 and 17, which show a high degree of consistency between the simulation and experimental results. To sum up, the SGPID control approach may improve the hydraulic actuator's dynamic performance, guaranteeing dependable synchronization control and deviation correction in the propulsion system.



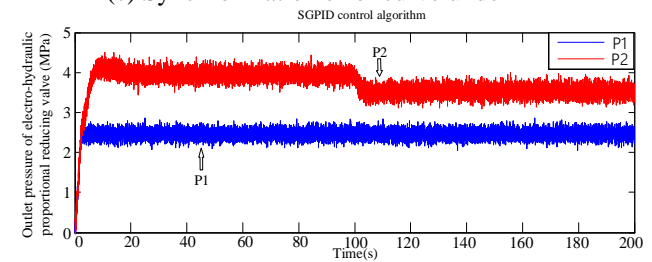
(a) Load loading curve



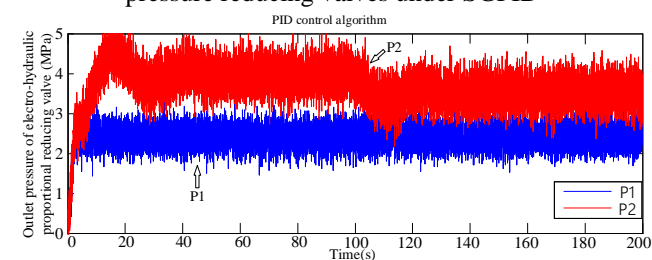
(b) Synchronization error curve under SGPID



(c) Synchronization error curve under PID



(d) Outlet pressure of electric-hydraulic proportional pressure reducing valves under SGPID



(e) Outlet pressure of electric-hydraulic proportional regulators under PID

Fig. 17. Synchronous experiment under partial load.

VII. CONCLUSION

- 1) A bond graph model for the synchronous control of the TBM propulsion system was developed based on the actual operating conditions of the system and in conjunction with the bond graph theory modeling method. The state space expression was derived, making computer simulation easier.
- 2) The grey prediction model is applied to traditional PID control in response to the electromechanical hydraulic coupling characteristics of the TBM propulsion system and the ambiguous external environmental information. To address the limitations of grey prediction adjustment mechanisms, a straightforward and useful step adjustment mechanism is suggested.
- 3) SGPID has excellent practical value and can increase the electro-hydraulic proportional synchronous control system's accuracy and reduce system fluctuations under the same PID parameter settings.
- 4) The accuracy of the TBM propulsion system's mathematical model was confirmed by contrasting the bond graph model's simulation and experimental outcomes.

REFERENCES

- [1] J. B. Li, "Current situation, problems and prospects of development of tunnel boring machines in China," *Tunnel Construction J.*, vol. 41, no. 4, pp. 877-896, Mar. 2021.
- [2] Z. G. Zhang, W. B. Ji, B. W. Yang, et al., "Dynamic analysis and vibration reduction of mechanical-hydraulic coupled tunnel boring machine (TBM) main drive system," *Proceedings of the Institution of Mechanical Engineers, Part C: Journal of Mechanical Engineering Science J.*, vol. 236, no. 1, pp. 115-125, Oct. 2021.
- [3] B. Deng, "Analysis of tunnel boring machine (TBM) drive system," *Equipment Management and Maintenance J.*, vol. 4, no. 3, pp. 136-138, Feb. 2020.
- [4] X. H. Li, H. B. Yu, M. Z. Yuan, et al., "Research on Dynamic Models and Performances of Shield Tunnel Boring Machine Cutterhead Driving System," *Advances in Mechanical Engineering J.*, vol. 5, no. 1, pp. 1-14, Aug. 2019.
- [5] Y. M. Xu, "Analysis and Design of Electro-hydraulic Proportional Control System," Machinery Industry Press M., 2005.
- [6] L. P. Wang, T. H. Peng, "Research on electro-hydraulic proportional height adjustment system based on single neuron PID control," *Coal Engineering J.*, vol. 51, no. 1, pp. 130-134, Feb. 2019.
- [7] H. J. Xiong, H. Z. Xu, "Grey control," National Defense Industry Press M., 2005.
- [8] J. L. Xiao, J. Ji, Y. S. Yao, et al., "Application of grey prediction in FAST hydraulic actuators," *Journal of Tianjin University: Natural Science and Engineering Technology Edition J.*, vol. 49, no. 2, pp. 178-185, Feb. 2016.
- [9] A. Kumar, A. S. Sidana, A. Kanda, V. Kumar and K. P. S. Rana, "Fuzzy controller with grey predictor for an inverted pendulum," 2016 IEEE 1st International Conference on Power Electronics, Intelligent Control and Energy Systems (ICPEICES), 2016, Delhi, India, pp 1-5.
- [10] J. Lin, H. Chiang, C. C. Lin, "Tuning PID control parameters for micro-piezo-stage by using grey relational analysis," *Expert Systems with Applications J.*, vol. 38, no.11, pp. 13924-13932, Oct. 2011.
- [11] E. Kayanan, O. Kaynak, "An adaptive grey PID-type fuzzy controller design for a nonlinear liquid level system," *Transactions of the Institute of Measurement and Control J.*, vol. 31, no. 1, pp. 33-49, Feb. 2009.
- [12] M. Luo, D. Wang, X. C. Wang, et al., "Analysis of Surface Settlement Induced by Shield Tunnelling: Grey Relational Analysis and Numerical Simulation Study on Critical Construction Parameters," *Sustainability J.*, vol. 15, no. 19, Sep. 2023.
- [13] JQ. T. Dinh, K. A. Kyoung, "Force control for hydraulic load simulator using self-tuning grey predictor – fuzzy PID," *Mechatronics J.*, vol. 19, no. 2, pp. 233-246, Mar. 2009.
- [14] J. L. Xiao, G. D. Wang, X. A. Yan, et al., "Switching grey prediction fuzzy control research and application," *Tianjin University J.*, vol. 40, no. 7, pp. 859-863, Jul. 2007.

- [15] H. Y. Yin, "Research on fuzzy control of a certain weapon depth determination system based on gray prediction with variable step size," Nanjing University of Science and Technology D., Jan. 2015.
- [16] Y. D. Pan, Q. Li, H. D. Li, "Electric Drive Automatic Control System," Machinery Industry Press M., 2014.
- [17] Wencheng Yu, "Object Tracking via Background-Aware Correlation Filter with Elliptical Search Area," *Engineering Letters*, vol. 31, no.4, pp1747-1758, 2023
- [18] K. Chen, L. F. Qian, X. P. Yu, et al., "Research on stochastic internal leakage model of external gear pump," *Chinese Journal of Computational Mechanics J.*, vol. 35, no. 6, pp. 782-788, Dec. 2018.
- [19] T. X. Lou, H. G. Ding, J. Dong, et al., "Design and Simulation Analysis of the Electrohydraulic Proportional Closed Loop Drive System for Coal Mine Hydraulic Winches," *Chinese Hydraulics & Pneumatics J.*, no. 6, pp. 63-68, Jun. 2019.
- [20] S. Pan, X. Luo, "Valve-controlled asymmetric cylinder position model reference adaptive control," 2022 IEEE 6th Advanced Information Technology, Electronic and Automation Control Conference (IAEAC), Beijing, China, 2022, pp. 338-343.
- [21] E. Giraldo, "Adaptive Model-based Control Design of a Synchronous Buck Converter," *Engineering Letters*, vol. 30, no.4, pp1364-1371, 2022
- [22] W. Mao, Z. K. Ji, H. L. Wei, et al., "Application Research of Fuzzy-PID Composite Control of Electro-hydraulic Proportional Servo System," *Chinese Hydraulics & Pneumatics J.*, no. 1, pp. 95-99, Jan. 2019.
- [23] J. Wang, W. J. Hu, S. X. Zhu, "Research on position control of electro-hydraulic proportional system based on virtual instrument," *Machine Tool and Hydraulics J.*, vol. 45, no. 5, pp. 86-90+118, Mar. 2017.
- [24] X. Li, "Research on Dead Zone Fuzzy Compensation Control of Electro-hydraulic Proportional Position Control System" *Internal Combustion Engine and Parts J.*, no. 18, pp. 110-111, Sep. 2018.
- [25] Zaiful Ulum, Salmah, Ari Suparwanto, and Solikhatus, "The Design of Coalitional Model Predictive Control for Large-Scale Systems," *Engineering Letters*, vol. 31, no.1, pp66-76, 2023
- [26] Yinghao Yang, Zhenle Dong, Zhigang Zhou, Zheng Zhang, Geqiang Li, and Yugong Dang, "RISE based Synchronous Control of Dual Electro-hydraulic Servo System via Internal Force Adjustment," *Engineering Letters*, vol. 30, no.3, pp1146-1151, 2022

**First Hanbing Zhang** graduated from Tianjin University with a Ph.D in Mechanical Engineering in 2016, and currently employed with Dalian Ocean University's School of Mechanical and Power Engineering. Principally involved in mechanical system dynamics, equipment technologies for fisheries and aquatic products processing. Serves as the Deputy Director of the Experimental Center in the School of Mechanical Engineering in Dalian Ocean University.